RSC Advances

ROYAL SOCIETY OF CHEMISTRY

www.rsc.org/advances

Magnetic mesoporous imprinted adsorbent based on Fe_3O_4–modified sepiolite for organic micropollutant removal from aqueous solution

Haicheng Liu [a,b], Wei Chen [a,*]

[a] *College of environment, Hohai University, Nanjing, 210098, PR China China*

[b] *Department of Environmental and Municipal Engineering, Henan University of Urban Construction, Pingdingshan, 467036, PR China*

***Corresponding author:** Tel: +86−25−83787618; E-mail: cw5826@hhu.edu.cn

Address for correspondence: Wei Chen, College of Environment, Hohai University, 1 Xikang Road, Nanjing, 210098, PR China.

Abstract: Magnetic molecularly imprinted polymer (MSEP@MIP) adsorbent was prepared by using magnetic Fe_3O_4–modified sepiolite (MSEP) particles as magnetic carrier for the efficient removal of herbicide atrazine from aqueous solution. The composition, thermal stability, chemical structure, specific surface area, morphology, and magnetic property of MSEP@MIP adsorbent were characterized by X–ray diffraction (XRD), thermal-gravimetric analyzer (TGA), Fourier transform infrared spectra (FTIR), Brunauer–Emmett–Teller (BET) method, scanning electron microscope (SEM) and vibrating sample magnetometer (VSM), respectively. The absorption isothermal and kinetics experiments were employed to investigate the adsorption capacity of atrazine onto MSEP@MIP. The prepared MSEP@MIP adsorbent was mesoporous. Compared with magnetic non–imprinted polymer (MSEP@NIP) and MSEP, MSEP@MIP showed greater removal efficiency for atrazine (about 91.3% for an initial concentration of 0.1 mg L^{-1}). Kinetic studies depicted that the adsorption process onto MSEP@MIP followed

pseudo-second-order rate equation. Isotherm studies indicated that the atrazine adsorption onto MSEP@MIP was monolayer molecular adsorption with a maximum adsorption amount of 69.53 mg g^{-1}. Scatchard analysis showed that there are two kinds of different binding sites in MSEP@MIP. Furthermore, the thermodynamics parameters indicated that the reaction between MSEP@MIP and atrazine was physical, exothermic, and nonspontaneous in nature.

Keywords: Atrazine, Organic micropollutant, Magnetic molecularly imprinted polymer, Removal, Sepiolite

1. Introduction

Recent years, many kinds of synthesized chemicals such as pharmaceuticals and personal care products, herbicide and pesticide were frequently detected in ground, surface and drinking waters.[1-3] Because of low concentration in water (μg L^{-1} or ng L^{-1} order of magnitude) and low removal efficiency for conventional water treatment processes,[4] effective removal of organic micropollutants from environmental water samples is becoming a subject of worldwide concern.

Comparing to some advanced treatment techniques such as precipitation, ion–exchange, solvent extraction, and nanofiltration, adsorption technology has been regarded as a more efficient method to remove low concentrations of pollutants from water because of its high removal efficiency and no harmful by-product.[5] Except for active carbon,[6-8] many new adsorbents such as natural clays and their modified products,[9-11] biomaterials,[12] mineral materials,[13] and iron–exchange resin[14] have been applied to remove organic micropollutants from water and wastewater. However, the complication of real water samples such as high concentration of natural organic matter (NOM) will reduce the adsorption capacity of

micropollutants onto adsorbents.[6,10,15] Therefore, it is necessary to research new adsorbent for the removal of organic micropollutants in complicated water.

Molecularly imprinted polymer (MIP) was highly cross–linked polymer prepared by copolymerizing functional monomers and cross–linker in the presence of template molecule. Possessing high selectivity and affinity to the target molecule, the research and application about MIP have attracted considerable attention in many fields, such as chemosensor for selective detection of organic micropollutants,[16,17] preconcentration and separation of organic micropollutants,[18] photocatalytic degradation of organics,[19] and solid-phase extraction (SPE).[20,21]

However, the applications of most of these new adsorbents including MIP especially the nanoscale adsorbents have been inhibited by the difficulty in recovering adsorbents after adsorption applications due to their relatively small sizes.[5] Herein, recently, more focuses have been directed on fabricating magnetic molecularly imprinted polymer (MMIP), a novel molecularly imprinted polymer composite incorporated with magnetic particles, which could be easily separated from aqueous solution by the employment of magnetic process. Ji et al.[22] reported magnetic molecularly imprinted polymeric microspheres of bisphenol A with Fe_3O_4 being utilized as carrier and obtained a adsorption amount of 390 mg g^{-1} for bisphenol A. Dramou et al.[23] used Fe_3O_4 as magnetic component to prepare magnetic polymers for extraction of gatifloxacin from urine and lake water. Hiratsuka et al.[24] prepared magnetic molecularly imprinted polymers by a multi–step swelling and polymerization method using uniformly–sized magnetic particles, and used the MIPs to extract and determinate BPA in river water samples.

Gao et al.[25] synthesized thin imprinted shells over functionalized magnetic nanoparticles for specific removal of protein from bovine blood. Unfortunately, all the MMIPs discussed above were prepared using pure Fe_3O_4 particles as magnetic component, which must increase the cost of MMIP. Thus, many researches tried to use magnetic composites as the substitutions of Fe_3O_4 particles to synthesize MMIP. To date, very few magnetic composites such as Fe_3O_4@SiO_2 microspheres,[26,27] attapulgite@Fe_3O_4 particles,[28] magnetic yeast composites,[29] magnetic floating fly-ash cenospheres,[30] magnetic halloysite nanotubes[31] and TiO_2@Fe_3O_4 nanoparticles[32] have been used to prepare MMIPs for selective recognition and determination of micropollutants in aqueous solution. To our best knowledge, there is no research report on the preparation and application of MMIP based on Fe_3O_4–modified sepiolite (MSEP). MSEP is a fibrous hydrated magnesium silicate coated with magnetic Fe_3O_4 particles and a general structure formed by an alternation of blocks and tunnels that follow the fibre direction (c-axis). Each structural block occurs as a layer-chain structure that is composed of two tetrahedral silica sheets and an octahedral magnesia sheet. This unique fibrous structure allows penetration of organic and inorganic ions into the structure of MSEP and assigns MSEP an important role in sorptive and catalytic applications. [33]

Atrazine (ATZ), one of the triazine herbicides, is widely used around the world. Classified as a human carcinogenic compound, ATZ has been included in the priority substances list of the European Commission, United States Environmental Protection Agency and Ministry of Environmental Protection of China.[7,34] Furthermore, it has been reported that atrazine can cause biological effects of model animals even at much lower the regulated safe dose levels.[35]

European countries have set a severe concentration limit of 0.1 ppb for atrazine in surface and ground waters and the limit of 3 ppb in United States and China.[7,36] Therefore, ATZ was chosen as a model contaminant to investigate the adsorption capacity of organic micropollutants onto MSEP@MIP in the present study.

The aims of this study were as follows: (1) to prepare magnetic molecularly imprinted polymer adsorbent (MSEP@MIP) for the first time using MSEP as the magnetic carrier, (2) to investigate the basic chemical and physical characteristics of MSEP@MIP, including composition, specific surface area and pore character, thermal stability, chemical structure, magnetic property, and morphology by various instrumental analyses, (3) to evaluate the adsorption capacity and kinetics of atrazine onto MSEP@MIP with adsorption isotherm models, Scatchard model analysis and kinetic models.

2. Materials and methods

2.1. Materials

The natural sepiolite used in this study was obtained from Dongfeng Sepiolite Co., Ltd. (Xinyang, China). Ferric chloride ($FeCl_3 \cdot 6H_2O$), ferrous sulfate ($FeSO_4 \cdot 7H_2O$), sodium hydroxide (NaOH) and ammonium hydroxide ($NH_4 \cdot OH$) were purchased from Kelong Chemical Co., Ltd. (Chengdu, China). Methacrylic acid (MAA), azobisisobutyronitrile (AIBN), ethylene glycol dimethacrylate (EGDMA), methyl sulfoxide (DMSO), polyvinyl Pyrrolidone (PVP) were all purchased from Aladdin reagent CO., LTD. (Shanghai, China).

High purity (99.1%) ATZ was purchased from Oddfoni Biological Technology Co., Ltd. (Nanjing, China). ATZ stock solution (500 mg L^{-1}) was prepared using a mixture solvent of

ethanol and distilled water (1:1, v/v) and was used for all the adsorption experiments after necessary dilutions with distilled water. All other reagents were of analytical grade and all the reagents were used as received without further purification.

2.2. Preparation of adsorbent

2.2.1. Preparation of MSEP carrier

MSEP used in this study was prepared and evaluated according to the method reported by Liu et al.[36] previously in our lab.

2.2.2. Preparation of MSEP@MIP

The MSEP@MIP materials were synthesized as follows procedure. First, ATZ (215.7 mg) and MAA (0.5 mL) were dispersed into the 10 mL of DMSO in ultrasonic bath at 40 °C for 0.5 h. Second, MSEP particles (1.0 g, with a particle size of 200–mesh) was dispersed with 4 mL of DMSO under ultrasound at 40 °C for 15 min in a 50–mL beaker. Then 3.8 mL of EGDMA and the self–assembly solution were both added into the flask and this mixture was sonicated again for 30 min. Third, PVP (0.5 g) was dissolved into 100 mL of DMSO/H_2O (9:1, v/v) in a three–necked round–bottomed flask and stirred (250 ±10 rpm) under the protection of N_2 at 70 °C for 15 min in a thermostatic water bath. The prepolymerization solution was then transferred into the three–necked flask followed by the addition of AIBN (0.1 g). The whole mixture solution was stirred again for 30 min under N_2 atmosphere. After that, the stirring speed was increased to 450 ±10 rpm, and the reaction was maintained without the protection of N_2 at 70 °C for 12 h.

Upon completion of the polymerization, the obtained products were collected by permanent

magnet and washed with ethanol and distilled water three times. After that, Soxhlet extraction technology was employed to removal the template molecules (ATZ) with a mixture of methanol/acetic acid (9:1, v/v) at 80 °C for 24 h. Finally, the obtained MSEP@MIP materials were washed with ethanol and distilled water to remove the remaining acetic acid and dried for 24 h under vacuum at 60 °C. As a control, magnetic non–imprinted polymer (MSEP@NIP) was also prepared using the same procedure but without adding atrazine template.

2.3. Apparatus and characterizations

X–ray diffraction (XRD) patterns were recorded on an XPert pro X–ray diffractometer (PANalytical, Holland) using CuKa radiation at a scanning speed of 2° min^{-1} over 2θ from 5° to 80° operated at 40 kV and 40 mA. Thermogravimetric analysis (TGA) curves were obtained by heating the sample in a platinum cell from 25 to 800 °C at a heating rate of 20 °C/min under a N_2 atmosphere using a thermogravimetric analyzer (PerKinElmer, USA). Fourier transform infrared spectra (FTIR) were recorded at 400–4000 cm^{-1} using a NEXUS870 Fourier Transform Infrared Spectrometer (Nicolet, USA). Nitrogen adsorption-desorption isotherms at 77 K were obtained using a Micrometrics ASAP 2020 analyzer (Micromeritics, USA). Based on the N_2 adsorption isotherm data, the specific surface areas and the pore diameter distributions were calculated according to the Brunauer–Emmett–Teller (BET) method and the Barret–Joyner–Halenda (BJH) method, respectively. The surface morphologies were examined using a Hitachi S–4800 scanning electron microscope (SEM) with an accelerating voltage of 5 kV. The saturation magnetization values (Ms) of materials were obtained from their magnetic hysteresis loops which were recorded by a 7404 vibrating sample magnetometer (Lakeshore,

USA) at room temperature.

2.4. Adsorption experiment

A mass of 20 mg of adsorbent was added into 100–mL stoppered conical flasks containing 50 mL of ATZ solution. The pH of solution was adjusted using 0.1 mol L^{-1} HCl or NaOH solutions. The mixture was agitated in a temperature–controlled shaking water bath with a constant speed of 180 rpm. In the kinetic adsorption experiments, 0.1 mg L^{-1} ATZ solution was used. In the adsorption equilibrium experiments, the initrial concentration of ATZ varied from 0.01 mg L^{-1} to 50 mg L^{-1}. Upon completion of adsorption, the mixture was magnetic separation by a magnet and the supernatant was filtered with 0.45–μm filter. The residual ATZ concentration in the filtrate was detected with HPLC. The ATZ removal efficiency and ATZ uptake amount onto adsorbent were determined using the following equations:

$$\text{Removal efficiency}\,(\%) = \frac{C_0 - C_e}{C_0} \times 100 \qquad (1)$$

$$q_e = \frac{(C_0 - C_e) \times V}{m} \qquad (2)$$

where C_0 and C_e represent the initial and equilibrium concentrations (mg L^{-1}), respectively. q_e (mg g^{-1}) is the adsorption amount of ATZ onto adeorbent. V (L) is the volume of the solution and m (g) is the mass of adsorbent added. All tests were performed in triplicate to insure the reproducibility of the results, and the average values were reported with error bars representing standard dev170iations.

In order to estimate the selectivity of MSEP@ MIP for ATZ, 20 mg MSEP@ MIP was dispersed into 50 mL of aqueous solutions containing 0.1 mg L^{-1} of ATZ, cyanazine and

melamine respectively. The mixture was shaken in a temperature–controlled shaking water bath with a constant speed of 180 rpm at 25 °C for 180 min. The residual concentrations of ATZ, cyanazine and melamine were determined by HPLC.

2.5. Model analysis

The experimental data that were obtained from the kinetic study were fit to pseudo-first-order (Eq. (3)) and pseudo-second-order (Eq. (4)) rate equations.[37]

$$q_t = q_e(1 - e^{-k_1 t}) \quad (3)$$

$$q_t = \frac{k_2 q_e^{\,2} t}{1 + k_2 q_e t} \quad (4)$$

where q_e and q_t are the amount of adsorbate (mg g^{-1}) onto adsorbent at the equilibrium and any time t (min), respectively. k_1 (min^{-1}) and k_2 (g mg^{-1} min^{-1}) are the kinetic constant.

Furthermore, the experimental data that were obtained from the equilibrium study were fitted to Langmuir (Eq. (5)), Freundlich (Eq. (6)), Temkin (Eq. (7)) and Dubinin–Radushkevich (D–R) (Eq. (8)) isotherm models.[38]

Langmuir isotherm model:

$$q_e = \frac{q_m K_L C_e}{1 + K_L C_e} \quad (5)$$

where q_m (mg g^{-1}) is the maximum adsorption capacity of the adsorbent, and K_L (L mg^{-1}) represents the affinity constant. For predicting the favourability of an adsorption system, the Langmuir equation can also be expressed in terms of a dimensionless separation factor R_L which is related to the Langmuir constaint (K_L) and the maximal initial concentration of adsorbate (C_{0m}, mg L^{-1}). R_L equals to $1/(1+ K_L \cdot C_{0m})$, and when $0 < R_L < 1.0$, it represents a good adsorption.

Freundlich isotherm model:

$$q_e = K_F C_e^{1/n} \quad (6)$$

where K_F ($mg^{1-1/n}$ $L^{1/n}$ g^{-1}) is an indicative constant for adsorption capacity of the adsorbent and the constant $1/n$ indicates the intensity of the adsorption. Value of $1/n$ ranging from 0.1 to 1.0 represents a favourable adsorption condition.

Temkin isotherm model:

$$q_e = \frac{RT}{b}(\ln K_t + \ln C_e) \quad (7)$$

where b (J mol^{-1}) is the Temkin constant related to the heat of adsorption, K_t (L mol^{-1}) is the Temkin isotherm constant corresponding to maximum binding energy, R is the gas constant (8.314 J mol^{-1} K^{-1}) and T (K) is absolute temperature.

Dubinin–Radushkevich (D–R) isotherm model:

$$q_e = q_m \cdot \exp(-\beta\varepsilon^2) \quad (8)$$

where q_m (mg g^{-1}) is the the maximum adsorption amount, ε is the Polanyi potential which equals to $RT\ln(1+(1/C_e))$, β is the constant related to free energy (E), and E (J mol^{-1}) equals to $1/(2\beta)^{0.5}$.

2.6. Analysis of atrazine

In order to prevent aerobic biodegradation and photochemical decomposition of atrazine, some measures provided by a previous literature were performed during all the adsorption expetiments.[36] The atrazine concentrations in aqueous solutions were measured using high performance liquid chromatography (HPLC, Alliance 2695, Waters Co., America) equipped with a C18 column (5 μm, 4.6×250 mm, Waters Co.) and detected by UV spectrophotometry

(2487 2–Channel UV/VIS detector, Waters Co.) at a wavelength of 220 nm. The mobile phase of acetonitrile/water mixture (60:40, V/V) was used at a flow rate of 1 mL min^{-1} and the injection volume was set at 20 μL. Furthermore, the operating temperature and pressure were 30 °C and 62 bar, respectively.

2.7. Chi–square test

The Chi–square test was employed to measure the difference between the experimental and model data. The mathematical form of this test statistic can be expressed as:

$$\chi^2 = \sum \frac{(q_{e,exp} - q_{e,cal})^2}{q_{e,cal}} \qquad (9)$$

where $q_{e,exp}$ is the experimental equilibrium adsorption capacity and $q_{e,cal}$ is the adsorption equilibrium capacity from a model. If data from the model are similar to experimental data, χ^2 will be small and if they differ, χ^2 will be large. In order to confirm the best-fit kinetic model for the adsorption system, there is a need to analyse the data set using the Chi-square, combined with the values of the correlation coefficient (R^2).

2.8. Regeneration and reuse of adsorbent

To evaluate the reusability of the adsorbent, desorption of ATZ and regeneration of spent adserbents were performed in seven consecutive cycles. In each cycle, 50 mL of ATZ solution (0.1 mg L^{-1}, pH 6.5) was mixed with 0.02 g adseorbents for 3 h. After magnetic separation, the supernatant was subjected to ATZ measurement and the spent adsorbents were mixed with 20 mL of regenerant solution composed of methanol and distilled water (9:1, v/v) and shaked for 12 h in a temperature–controlled water bath with a constant speed of 150 rpm at the temperature of 35 °C.

3. Results and discussions

3.1. Characterization of materials

3.1.1. XRD patterns

According to the patterns of MSEP and MSEP@MIP (Fig. 1), the peaks at 2θ = 7.30°, 11.84°, 19.71°, 20.59°, 23.80°, 26.40°, 33.13°, and 60.90° correspond to the characteristic peaks of sepiolite (JCPDS card no. 13–0595).[36] Furthermore, six important diffraction peaks of Fe_3O_4 crystalline (JCPDS card no. 65–3107) at 2θ = 30.39° (220), 35.56° (311), 43.29° (400), 53.57° (422), 57.37° (511), and 63.04° (440) are observed in the patterns of MSEP and MSEP@MIP, indicating that the crystalline structure of the MSEP kept no change during the polymerization reaction. The analogous results have been reported by Li et al.[26] and Pan et al.[28] when they prepared magnetic imprinted materials using Fe_3O_4@SiO_2 and attapulgite@Fe_3O_4 particles as carrier, respectively.

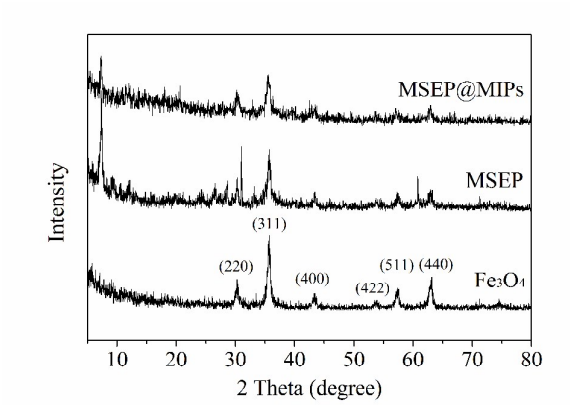

Fig. 1 XRD patterns of Fe_3O_4, MSEP and MSEP@MIP.

3.1.2. Thermal stability analysis

The TGA curves of MSEP and MSEP@MIP are given in Fig. 2. For MSEP (Fig. 2a), there are two major decomposition temperature regions. The initial weight loss of 3.06% from room

temperature (25 °C) to 130 °C corresponds to the release of adsorbed water. The second weight loss of 4.13% from 200 °C to 700 °C is caused by the loss of the hydroxyl group in structure of sepiolite. Form Fig. 2b, MSEP@MIP has also two stages of weight loss: the first (25–100 °C) is the loss of adsorbed water, which contributes the weight loss of 8.20%. The second (250–600 °C) exhibits the major weight loss of 69.08%, which is due to the thermal decomposition of the imprinted polymer on the surface of MSEP@MIP. Based on the weight loss obtained from the TGA analysis, it demonstrated that imprinted polymer has been successfully coated onto MSEP, and the polymer content is estimated as high as 69.08%.

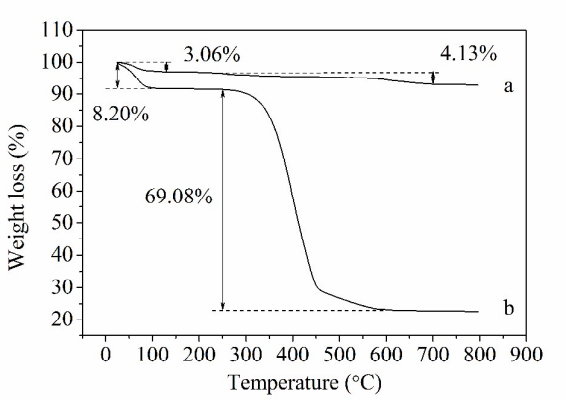

Fig. 2 TGA curves of MSEP (a) and MSEP@MIP (b).

3.1.3. FTIR spectra

The FTIR spectra of MSEP (a) and MSEP@MIP (b) are shown in Fig. 3. The characteristic absorption peaks around 3690 cm^{-1}, 3440 cm^{-1}, 1640 cm^{-1}, 1040 cm^{-1}, 975 cm^{-1}, 586 cm^{-1}, 467 cm^{-1} and 442 cm^{-1} are observed in all spectra of MSEP and MSEP@MIP. The band at 3690 cm^{-1} is assigned to stretching vibrations of hydroxyl groups attached to octahedral Mg^{2+} ions located in the interior blocks of sepiolite.[33] The peaks at 3440 cm^{-1} and 1640 cm^{-1} might be related to the stretching vibration of O–H bond and the bending vibration of H–O–H from water

molecules which were adsorbed on the external surface of the samples during handling to record the spectra.[39] The peaks at 1040 cm^{-1} and 975 cm^{-1} represent the stretching of Si-O in the Si–O–Si groups of the tetrahedral sheets of sepiolite.[33,40] The absorption band at 586 cm^{-1} corresponds to the stretching vibrations of Fe–O bond for spinel Fe_3O_4 particles, and the peaks at 467 cm^{-1} and 442 cm^{-1} are attributed to O–Si–O bending and Si–O–Mg bonds, respectively.[36,41]

From the spectrum of MSEP@MIP, the peaks at 2986 cm^{-1} and 2955 cm^{-1} indicate the presence of C–H stretching bands of both $–CH_3$ and $–CH_2$ groups.[28] The strong absorption bands at around 1725, 1260 and 1160 cm^{-1} are assigned to C=O stretching vibration of carboxyl (MAA), C–O symmetric and asymmetric stretching vibration of ester (EGDMA), respectively.[28] In addition, the absorption band at 1561 cm^{-1} is related to the characteristic absorption of carbonyl groups.[26] All the results confirmed that the copolymer of MAA and EGDMA has been coated on the surface of MSEP in the presence of AIBN as initiator, while the basic structure of MSEP has not been destroyed.

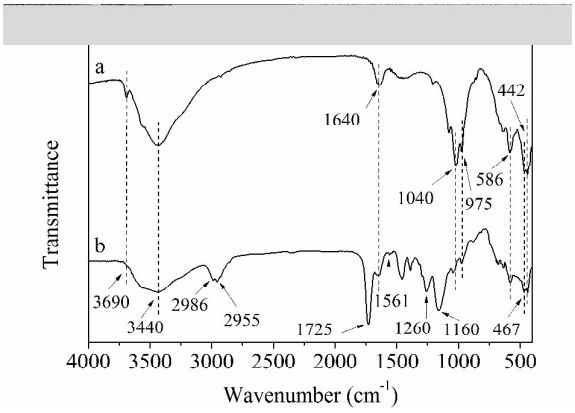

Fig. 3 FTIR spectra of MSEP (a) and MSEP@MIP (b).

3.1.4. BET analysis

Surface area and pore size of adsorbents are among important parameters that describe quality of adsorbents as they affect directly their analyte retention abilities. Fig. 4 shows the N_2 adsorption-desorption isotherm and the BJH pore size distribution of MSEP@MIP. From Fig. 4, MSEP@MIP is mainly mesoporous in nature with physisorption isotherm of Type IV and H_3 hysteresis loop features according to IUPAC classification,[36] which can be confirmed by the pore size distribution of MSEP@MIP (see the inset of Fig. 4). Table 1 summarizes the values of specific surface area, pore size and pore volume. As shown in Table 1, the specific surface area, average pore size and pore volume of MSEP@MIP was calculated at of 52.313 m^2 g^{-1}, 13.696 nm and 0.1791 cm^3 g^{-1} by means of BET and BJH method. The specific surface area and total pore volume dropped 53.5% and 26.5%, respectively, while the average pore size has a increasing of 58%. This may be due to the coating of copolymer on the surface of MSEP, which obstruct some of the main pore channels of MSEP, thus impeding the diffusion of N_2 throughout these channels.

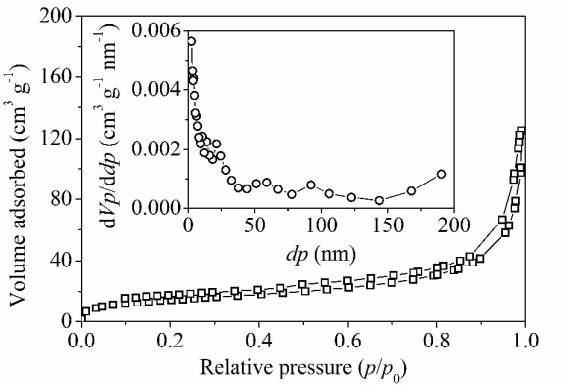

Fig. 4 N_2 adsorption/desorption isotherms (a), and BJH pore size distributions (b) of samples.

Table 1 Specific surface area, average pore size and total pore volume of samples.

Sample	Specific surface	Average pore size	Total pore volume	Reference

	area (m^2 g^{-1})	(nm)	(cm^3 g^{-1})	
MSEP	112.44	8.6703	0.2437	36
MSEP@MIP	52.313	13.696	0.1791	This work

3.1.5. Morphological characteristics

The morphologies of MSEP and MSEP@MIP were studied by SEM. The micrographs obtained for these materials are shown in Fig. 5. As seen in Fig. 5, the morphologies of the two samples are significantly different. In the MSEP microphotograph (Fig. 5a), the magnetic particles are much smaller, single magnetic particles or small aggregates of magnetic particles can be clearly observed along with the sepiolite fibers. In contrast, from the MSEP@MIP microphotograph (Fig. 5b), single magnetic particles can not be observed on the surface of fibers. Some large aggregates are obtained and the surface of the aggregates becomes smooth, which was originated from the formation of imprinted polymer on the surface of MSEP@MIP. Hence, the results fully demonstrated the existence of imprinted polymer.

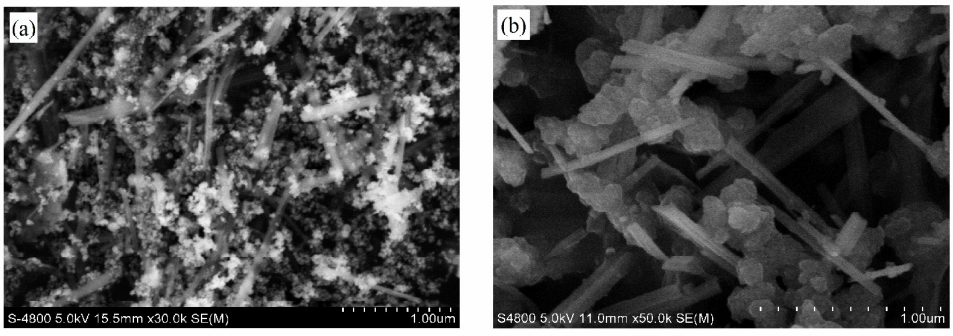

Fig. 5 SEM images of MSEP (a) and MSEP@MIP (b).

3.1.6. Magnetic property analysis

VSM was employed to study the magnetic properties of materials and the magnetic hysteresis loop of the samples is illustrated in Fig. 6. It can be seen that the shape and trend of the hysteresis loop of MSEP@MIP is similar to that of MSEP. The Ms value of MSEP@MIP obtained at room temperature is 18.43 emu g^{-1}, which is lower than that of MSEP.[36] The coating of polymer resulted in the reduction of saturation magnetization, but this was insignificant for MSEP@MIP to separate rapidly from mixture solution in an external magnetic field (see the inset of Fig. 6). In the absence of an external magnetic field, a brown homogeneous dispersion solution exists. When an external magnetic field was applied, the brown particles are attracted to the wall of vial in a short time (less than 30 s).

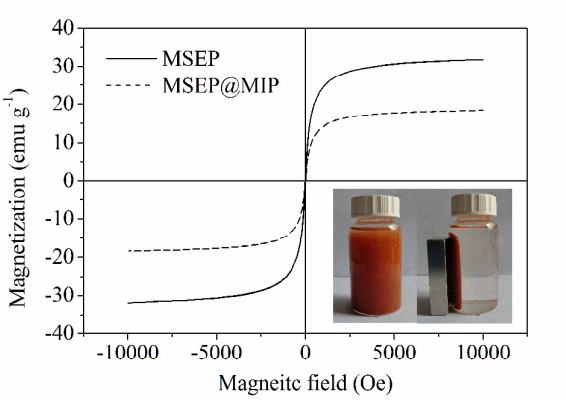

Fig. 6 Hysteresis loop of samples and photographs about magnetic response of MSEP@MIP in an external magnetic field.

3.2. Adsorption capacity of ATZ

3.2.1. Adsorption kinetics

Figure 7 shows the effect of contact time to ATZ adsorption onto MSEP@MIP and the plots of non–linear fitting of kinetics models. The corresponding kinetic parameters are summarized in Table 2. Compared to the pseudo–first–order model, the correlation coefficients (R^2) of

pseudo–second–order kinetic model were slightly high, while the Chi–square values (χ^2) were slightly low. In addition, the theoretical q_e values calculated from the pseudo–second–order kinetic model were closer to the experimental q_e values than that calculated from the pseudo–first–order kinetic model. Hence, the adsorptions of ATZ onto these materials were all considered to obey pseudo–second–order kinetic model rather than the pseudo–first–order one.

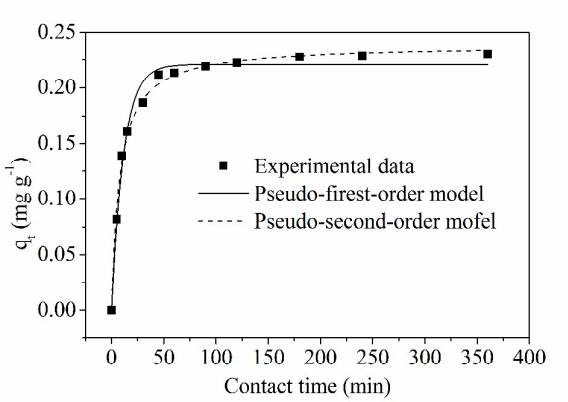

Fig. 7 Adsorption kinetics of ATZ and non-linear fitting of kinetic models.

Table 2 Adsorption kinetic parameters for adsorption of ATZ onto MSEP@MIP particles. (Conditions: adsorbent dosage = 0.4 g L^{-1}, C_0 = 0.1 mg L^{-1}, T = 25 °C, pH = 6.5)

Adsorbent	$q_{e,exp}$ †	Pseudo–first–order				Pseudo–second–order			
	(mg g^{-1})	$q_{e,cal}$ ‡ (mg g^{-1})	k_1 (min^{-1})	R^2	χ^2 (×10^{-3})	$q_{e,cal}$ (mg g^{-1})	k_2 (g mg^{-1} min^{-1})	R^2	χ^2 (×10^{-3})
MSEP@MIP	0.23	0.221	0.088	0.986	1.5	0.238	0.5384	0.995	1.2

† Equilibrium adsorption capacity obtained from experiments

‡ Theoretical equilibrium adsorption capacity calculated from kinetic model

3.2.2. Adsorption isotherm and Scatchard analysis

The adsorption isotherms of ATZ onto MSEP@MIP, MSEP@NIP and MSEP are presented in Fig. 8. From Fig. 8a, the amount of adsorbed ATZ onto three materials at equilibrium increase with the increasing of initial concentration of ATZ. However, the amount of ATZ adsorbed onto MSEP@MIP is much higher than that adsorbed onto MSEP@NIP and MSEP, displaying the molecular imprinting effect.

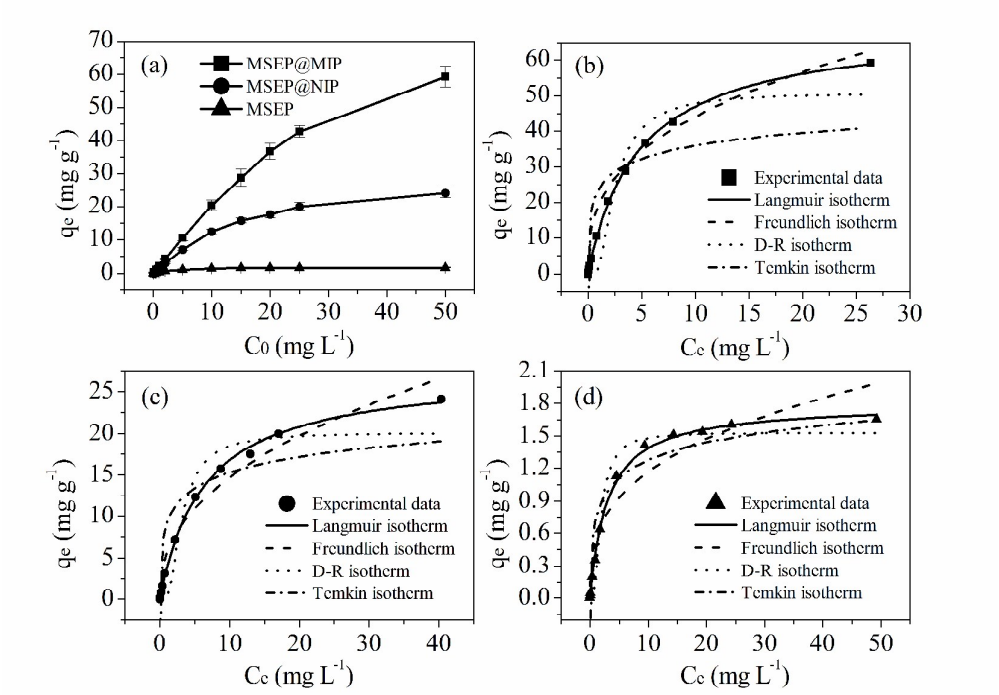

Fig. 8 Effect of initial concentration on adsorption (a), comparison of Langmuir, Freundlich, D–R and Temkin isotherm models for ATZ adsorption onto MSEP@MIP (b), MSEP@NIP (c) and MSEP (d).

The equilibrium data were analyzed using Langmuir, Freundlich, Temkin and D–R isotherm models (Fig. 8b–d), and all the calculated values of the adsorption isotherm parameters are listed in Table 3. It was found that Langmuir isotherm model fitted the equilibrium data

significantly better than that of the other three models for the high value of the correlation coefficients (R^2), indicating monolayer molecular adsorption for MSEP@MIP, MSEP@NIP and MSEP. Similar results were observed in the selective recognition of 2,4–dichlorophenol from aqueous solutions.[28] From Table 3, the maximum adsorption capacity predicted according to the Langmuir isotherm was 69.53, 27.51 and 1.8 mg/g at 25 °C for MSEP@MIP, MSEP@NIP and MSEP, respectively. In addition, the values of free adsorption energy, E, were all lower than 8 KJ/mol, suggesting a physical nature for ATZ adsorption onto the three materials.[42]

Table 3 Isotherm parameters for adsorption of ATZ onto MSEP@MIP, MSEP@NIP and MSEP. (Conditions: adsorbent dosage = 0.4 g L^{-1}, t =180 min, T = 25 °C, pH = 6.5)

Adsorption isotherm		Adsorbent		
Model	Parameter	MSEP@MIP	MSEP@NIP	MSEP
Langmuir	q_m (mg g^{-1})	69.53	27.51	1.8
	K_L (L mg^{-1})	0.2084	0.1554	0.3335
	R_L	0.0876	0.1140	0.0566
	R^2	0.9995	0.9984	0.9979
Freundlich	K_F ($mg^{1-1/n}$ $L^{1/n}$ g^{-1})	15.28	5.4831	0.5467
	$1/n$	0.4359	0.427	0.3306
	R^2	0.9661	0.9653	0.9117
D–R	q_m (mg g^{-1})	50.84	20.11	1.532
	β (mol^2 kJ^{-2})	1.09×10^{-6}	1.56×10^{-6}	6.21×10^{-7}
	E (kJ mol^{-1})	0.676	0.565	0.897

	R^2	0.9311	0.9383	0.9697
	K_t(L g^{-1})	89.12	30.69	22.94
Temkin	b (J mol^{-1})	468	929	10570
	R^2	0.7143	0.7963	0.8902

According to the adsorption equilibrium analysis as above, MSEP@MIP shows greater adsorption capacity for ATZ (69.53 mg g^{-1}) compared to MSEP@MIP (27.51mg g^{-1}) and MSEP (1.8 mg g^{-1}). In order to further study the binding properties of materials, Scatchard analysis was performed by using the equilibrium adsorption data. The value of maximum apparent adsorption amount, q_{max} (mg g^{-1}), was obtained by using Eq. (10).

$$\frac{q_e}{C_e} = \frac{q_{max} - q_e}{K_{di}} \qquad (10)$$

where K_{di} (mg L^{-1}) is the dissociation constant of binding sites.

It can be seen in Fig. 9, the relationship between q_e/C_e and q_e for MSEP@MIP could be expressed using two straight lines, which illustrated that two kinds of different binding sites existed in MSEP@MIP. The linear equations corresponding to two linear relationships were q_e/C_e = 28.24−5.74q_e (concentration range 0.01–1 mg g^{-1}) and q_e/C_e =15.69−0.2366q_e (concentration range 2–50 mg g^{-1}). The K_{di} and q_{max} were calculated from the slops and intercepts, and they were 0.1742 mg L^{-1} and 4.92 mg g^{-1} for the high affinity sites, and 4.227 mg L^{-1} and 66.32 mg g^{-1} for the low affinity sites, respectively.

In comparison, the binding characters of ATZ onto MSEP@NIP and MSEP were also analyzed by Scatchard method. As shown in Fig. 9, the relationship between q_e/C_e and q_e is a

single linear curve not only for MSEP@NIP but also for MSEP. The linear relationship can be expressed as q_e/C_e =4.799−0.1843q_e for MSEP@NIP and q_e/C_e =0.5455−0.2952q_e for MSEP. It revealed homogeneous binding sites with K_d and q_{max} values of 5.426 mg L^{-1} and 26.04 mg g^{-1} for MSEP@NIP, and 3.3875 mg L^{-1} and 1.8479 mg g^{-1} for MSEP. All the values of q_{max} show good agreement to the results of Langmuir isotherm.

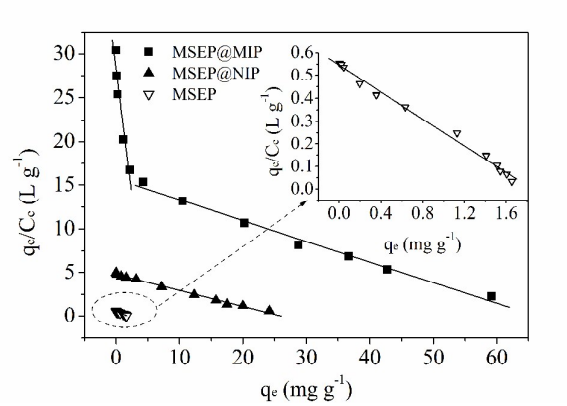

Fig. 9 Scatchard plots of MSEP@MIP (a), MSEP@NIP (b) and MSEP (c).

3.2.3. Adsorption thermodynamics

Thermodynamic parameters such as change in Gibbs free energy (ΔG°, kJ mol^{-1}), enthalpy (ΔH°, kJ mol^{-1}) and entropy (ΔS°, J mol^{-1} K^{-1}) were calculated at different temperatures (5, 15, 25, 35 °C) to evaluate the feasibility of the adsorption process. The values of ΔG° were calculated by the following equation:[38]

$$\Delta G^\circ = -RT \ln K_L \qquad (11)$$

where K_L is the Langmuir equilibrium constant (L mol^{-1}). The ΔH° and ΔS° were determined from the slope and intercept of the plot of ln(K_L) versus 1/T according to the Eq. (10):

$$\ln K_L = \frac{\Delta S^\circ}{R} - \frac{\Delta H^\circ}{RT} \qquad (12)$$

The thermodynamic parameters calculated are shown in Table 4. The positive values of ΔG°

at all temperatures indicated that the adsorption reaction was not a spontaneous one and that the system gained energy from an external source. The negative $\Delta H°$ value confirmed that the adsorption is an exothermic and stable process,[43] suggesting that the ATZ adsorption by MSEP@MIP decreases with an increase in the temperature. The same phenomenon was observed by Rambabu et al.,[7] who used granulated actived carbon to adsorb ATZ from aqueous solution. This can be explained that the mobility of atrazine molecules increased with increasing temperature, which leads to the weak forces more weakened with further increasing temperature, resulting in a decrease in the adsorption capacity of adsorbents.[36] The small negative value of $\Delta H°$ indicated that the adsorption is physical in nature involving weak forces of attraction, implying that there was loose bonding between the adsorbate molecules and the adsorbent surface,[44] which is favorable to desorb the adsorbate molecules when adsorbants need to be regenerated. The negative $\Delta S°$ suggested the drop in the degree of freedom by the adsorbed species. It also indicated that there is no structural change at solid–liquid interface and the adsorption process looks stable.[45] Furthermore, a greater value of $\Delta S°$ (> -10 J mol^{-1}) implied a dissociative mechanism of adsorption of ATZ onto MSEP@MIP adsorbent.[46]

Table 4 Thermodynamic parameters for adsorption of ATZ onto MSEP@MIP particles (Conditions: adsorbent dosage = 0.4 g L^{-1}, C_0 = 0.1 mg L^{-1}, t =180 min, pH = 6.5).

Temperature (°C)	$\Delta G°$ (kJ mol^{-1})	$\Delta H°$ (kJ mol^{-1})	$\Delta S°$ (J mol^{-1} K^{-1})
5 °C	2.747	−2.988	−8.257
15 °C	3.196		

25 °C	3.886
35 °C	4.352

3.3. Competitive adsorption, regeneration and reuse of MSEP@MIP

To further investigate the selective recognition properties of the MSEP@ MIP, the structurally similar compound cyanazine and melamine were selected to act as the competitors of ATZ. As can be seen from Fig. 10a, the removal efficiencies for ATZ, cyanazine and melamine by MSEP@ MIP were 83.19%, 54.54% and 43.51%, respectively, showing that MSEP@ MIP had the highest molecular recognition selectivity to ATZ. Compared with MSEP@ MIP, the adsorption selectivity of MAEP@NIP and MSEP is low.

According to the thermodynamic analyses, a greater temperature was unfavorable to ATZ adsorption from aqueous solutions by MSEP@MIP. Hence, the stability and potential regeneration/reuse of the MSEP@MIP adsorbent was investigated at a temperature of 35 °C with a regenerant composed for methanol and distilled water (9:1, v/v). Removal efficiencies of repeating application of MSEP@MIP are shown in Fig. 10b. After seven cycle's regeneration, the removal efficiency of MSEP@MIP for ATZ dropped about 6 % in ATZ solution (initial concentration 0.1 mg L^{-1}), suggesting good regeneration/reuse ability of MSEP@MIP.

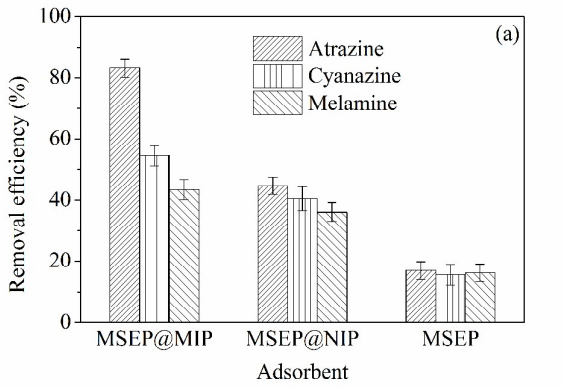

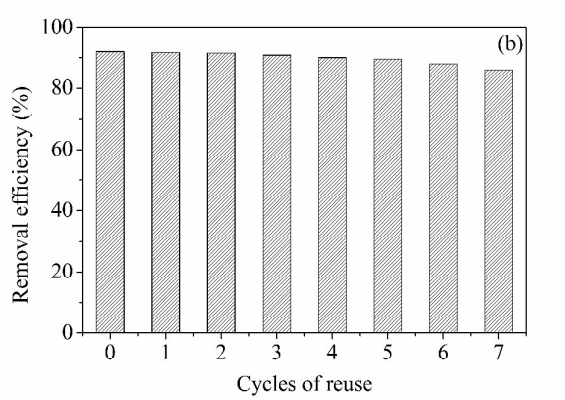

Fig. 10 Competitive adsorption of different molecules by MSEP@MIP, MSEP@NIP and MSEP (a), and regeneration and reuse of MSEP@MIP (b).

4. Conclusions

A novel magnetic adsorbent for organic micropollutant, prepared by using Fe_3O_4–modified sepiolite as magnetic carrier, atrazine as template molecule, methacrylic acid as functional monomer, ethylene glycol dimethacrylate as cross–linker and azobisisobutyronitrile as initiator, was used to analyze the removal efficiency of ATZ from surface water. The prepared MSEP@MIP possessed a specific surface area of 52.313 $m^2 g^{-1}$ and saturation magnetization of 18.43 emu g^{-1}. Batch experiments showed that the adsorption process fitted well with the pseudo–second–order kinetic model and could be best described by the Langmuir adsorption isotherm with a maximum uptake amount of 69.53 mg g^{-1}. Scatchard analysis implied that there existed two kinds of different adsorption sites in MSEP@MIP. Results showed that the MSEP@MIP was an effective adsorbent for ATZ adsorption and the adsorption process was exothermic and nonspontaneous. In addition, the involvement of magnetic component overcame the difficulty of separation of MIP particles from solution. Although the results reported here relate only to ATZ, the principles of the proposed methodology are expected to be applicable to

the removal of other organic micropollutants from contaminated water.

Acknowledgements

This study is financed by the National Natural Science Foundation of China (51178159) and the Postgraduate Technological Innovation Program of Jiangsu Province Education Department (CXZZ12_0236).

References

1 A. Murray and B. Ormeci, *Environ. Sci. Pollut. R.*, 2012, **19**, 3820.

2 S. W. Nam, B. I. Jo, Y.Yoon and K. D. Zoh, *Chemosphere*, 2014, **95**, 1565.

3 E. De Gerónimo, V. C. Aparicio, S. Bárbaro, R. Portocarrero, S. Jaime and J. L. Costa, *Chemosphere*, 2014, **107**, 423.

4 G. Buttiglieri, L. Migliorisi and F. Malpei, *Water Sci. Technol.*, 2011, **63**, 1334.

5 Y. J. Jin, F. Liu, M. P. Tong and Y. L. Hou, *J. Hazard. Mater.*, 2012, **227**, 461.

6 J. Y. Zhang, B. Y. Shi, T. Li and D. S. Wang, *Adsorption*, 2013, **19**, 91.

7 N. Rambabu, C. A. Guzman, J. Soltan and V. Himabindu, *Chem. Eng. Technol.*, 2012, **35**, 272.

8 J. L. Sotelo, G. Ovejero, A. Rodríguez, S. Álvarez and J. Garcia, *Chem. Eng. J.*, 2013, **228**, 102.

9 H. Azejjel, C. del Hoyo, K. Draoui, M. S. Rodriguez-Cruz and M. J. Sanchez-Martin, *Desalination*, 2009, **249**, 1151.

10 Y. P. Zhao, X. Y. Gu, S. X. Gao, J. J. Geng and X. R. Wang, *Geoderma*, 2012, **183-184**, 12.

11 R. Celis, M. A. Adelino, M. C. Hermosin and J. Cornejo, *J. Hazard. Mater.*, 2012, **209-210**, 67.

12 C. R. Silva, T. F. Gomes, G. C. R. M. Andrade, S. H. Monteiro, A. C. R. Dias, E. A. G. Zagatto and V. L. Tornisielo, *J. Agric. Food Chem.*, 2013, **61**, 2358.

13 M. Makehelwala, R. Weerasooriya, L. Jayaratne and C. B. Dissanayake, *J. Chem. Thermodynamics*, 2012, **51**, 1.

14 D. M. Jia, C. Zhou and C. H. Li, *Water Environ. Res.*, 2011, **83**, 784.

15 Y. Matsui, T. Yoshida, S. Nakao, D. R. U. Knappe and T. Matsushita, *Water Res.*, 2012, **46**, 4741.

16 B. W. Wu, L. J. Hou, M. Du, T. T. Zhang, Z. H. Wang, Z. H. Xue and X. Q. Lu, *RSC Adv.*, 2014, **4**, 53701.

17 W. R. Huang, Y. L. Chen, C. Y. Lee and H. T. Chiu, *RSC Adv.*, 2014, **4**, 62393.

18 S. F. Xu, J. H. Li and L. X. Chen, *Talanta*, 2011, **85**, 282.

19 W. N. Xing, L. Ni, X. L. Liu, Y. Y. Luo, Z. Y. Lu, Y. S. Yan and P. W. Huo, *RSC Adv.*, 2013, **3**, 26334.

20 L. Chimuka, M. van Pinxteren, J. Billing, E. Yilmaz and J. A. Jonsson, *J. Chromatogr. A*, 2011, **1218**, 647.

21 T. E. Milja, V. S. Krupa and T. P. Rao, *RSC Adv.*, 2014, **4**, 30718.

22 Y. S. Ji, J. J. Yin, Z. G. Xu, C. D. Zhao, H. Y. Huang, H. X. Zhang and C. M. Wang, *Anal. Bioanal. Chem.*, 2009, **395**, 1125.

23 P. Dramou, D. L. Xiao, H. He, T. B. Liu and W. Y. Zou, *J. Sep. Sci.*, 2013, **36**, 898.

24 Y. Hiratsuka, N. Funaya, H. Matsunaga and J. Haginaka, *J. Pharmaceut. Biomed.*, 2013, **75**, 180.

25 R. X. Gao, L. L. Zhang, Y. Hao, X. H. Cui and Y. H. Tang, *RSC Adv.*, 2014, **4**, 64514.

26 Y. Li, X. Li, J. Chu, C. K. Dong, J. Y. Qi and Y. X. Yuan, *Environ. Pollut.*, 2010, **158**, 2317.

27 R. X. Gao, Y. Hao, S. Q. Zhao, L. L. Zhang, X. H. Cui, D. C. Liu, Y. H. Tang and Y. S. Zheng, *RSC Adv.*, 2014, **4**, 56798.

28 J. M. Pan, L. C. Xu, J. D. Dai, X. X. Li, H. Hang, P. W. Huo, C. X. Li and Y. S. Yan, *Chem. Eng. J.*, 2011, **174**, 68.

29 X. X. Li, J. M. Pan, J. D. Dai, X. H. Dai, L. C. Xu, X. Wei, H. Hang, C. X. Li and Y. Liu, *Chem. Eng. J.*, 2012, **198-199**, 503.

30 Z. Y. Lu, Y. Y. Luo, M. He, P. W. Huo, T. T. Chen, W. D. Shi, Y. S. Yan, J. M. Pan, Z. F. Ma and S. Y. Yang, *RSC Adv.*, 2013, **4**, 18373.

31 J. D. Dai, X. Wei, Z. J. Cao, Z. P. Zhou, P. Yu, J. M. Pan, T. B. Zou, C. X. Li and Y. S. Yan, *RSC Adv.*, 2014, **4**, 7967.

32 S. F. Xu, H. Z. Lu, L. X. Chen and X. C. Wang, *RSC Adv.*, 2014, **4**, 45266.

33 S. Dikmen, G. Yilmaz, E. Yorukogullari and E. Korkmaz, *Can. J. Chem. Eng.*, 2012, **90**, 785.

34 Q. H. Wang, W. Zhang, C. Li and B. Xiao, *Water Sci. Technol.*, 2012, **66**, 1282.

35 J. Kaiser, *Science*, 2000, **290**, 695.

36 H. C. Liu, W. Chen, C. Liu, Y. Liu and C. L. Dong, *Micropor. Mesopor. Mater.*, 2014, **194**,

72.

37 A. Quek and R. Balasubramanian, *J. Colloid Interf. Sci.*, 2011, **356**, 203.

38 C. Y. Kuo, C. H. Wu and J. Y. Wu, *J. Colloid Interf. Sci.*, 2008, **327**, 308.

39 M. Salavati-Niasari, G. Hosseinzadeh and F. Davar, *J. Alloy. Compd.*, 2011, **509**, 134.

40 I. Kuncek and S. Sener, *Ultrason. Sonochem.*, 2010, **17**, 250.

41 S. Bakhtiary, M. Shirvani and H. Shariatmadari, *Micropor. Mesopor. Mater.*, 2013, **168**, 30.

42 P. Miretzky and C. Munoz, *Desalination*, 2011, **271**, 20.

43 N. Rauf, S. S. Tahir, J. H. Kang and Y. S. Chang, *Chem. Eng. J.*, 2012, **192**, 369.

44 A. Özcan, E. M. Öncü and A. S. Özcan, *Colloid. Surface. A*, 2006, **277**, 90.

45 B. Kakavandi, A. Esrafili, A. Mohseni-Bandpi, A. J. Jafari and R. R. Kalantary, *Water Sci. Technol.*, 2014, **69**, 147.

46 E. I. Unuabonah, G. U. Adie, L. O. Onah and O. G. Adeyemi, *Chem. Eng. J.*, 2009, **155**, 567.

Graphical abstract

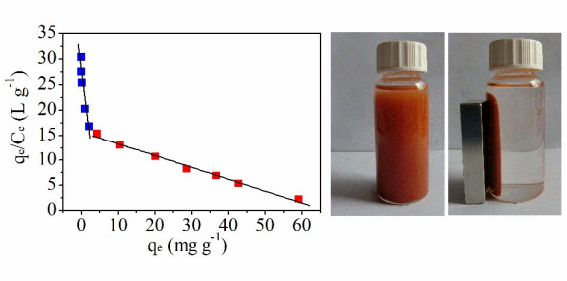

Novel magnetic molecularly imprinted polymer adsorbent based on magnetic sepiolite composite was successfully prepared for the first time. It has a maximum adsorption capacity of 69.53 mg g^{-1} for atrazine.